Chemistry & Biology, Vol. 9, 345–350, March, 2002, ©2002 Elsevier Science Ltd. All rights reserved. PII S1074-5521(02)00120-5

Direct Visualization of a DNA Glycosylase Searching for Damage

Liwei Chen,[2] Karl A. Haushalter,[2]
Charles M. Lieber,[1] and Gregory L. Verdine[1]
Department of Chemistry and Chemical Biology
Harvard University
12 Oxford Street
Cambridge, Massachusetts 02138

Summary

DNA glycosylases preserve the integrity of genetic information by recognizing damaged bases in the genome and catalyzing their excision. It is unknown how DNA glycosylases locate covalently modified bases hidden in the DNA helix amongst vast numbers of normal bases. Here we employ atomic-force microscopy (AFM) with carbon nanotube probes to image search intermediates of human 8-oxoguanine DNA glycosylase (hOGG1) scanning DNA. We show that hOGG1 interrogates DNA at undamaged sites by inducing drastic kinks. The sharp DNA bending angle of these nonlesion-specific search intermediates closely matches that observed in the specific complex of 8-oxoguanine-containing DNA bound to hOGG1. These findings indicate that hOGG1 actively distorts DNA while searching for damaged bases.

Introduction

DNA glycosylases are responsible for the recognition and removal of damaged bases from the genome [1]. Despite tremendous structural divergence among DNA glycosylases, all share the strikingly similar characteristic of repairing aberrant bases that are swiveled from the DNA helix and inserted into an extrahelical active site pocket on the enzyme [2]. In the absence of the enzyme, these substrate bases typically remain in the helix, where they are inaccessible to the glycosylase active site. These observations raise the puzzling question of how DNA glycosylases conduct an efficient search for damaged bases that are seemingly hidden amidst a 1,000,000-fold excess of normal bases. Insight into the search mechanism could be gained through an understanding of how glycosylases affect the structure of undamaged DNA. Conventional high-resolution structural techniques are ill-suited to this problem because these methods require homogeneous samples. Conversely, single-molecule imaging techniques can analyze individual members within a complex population of molecules [3] and thereby provide unique mechanistic insight. As illustrated in Figure 1, here we report the use of atomic-force microscopy (AFM) with single-walled carbon nanotube (SWNT) probes [4, 5] to probe the lesion-searching mechanism employed by the human 8-oxoguanine DNA glycosylase (hOGG1) [6].

[1]Correspondence: cml@cmliris.harvard.edu (C.M.L.)
verdine@chemistry.harvard.edu (G.L.V.)
[2]These authors contributed equally to this work.

The hOGG1 enzyme targets a highly mutagenic base lesion, 8-oxoguanine (oxoG), which arises in DNA through the attack of reactive oxidants on guanine residues. Mutation of Lys249, a key nucleophilic residue on hOGG1, to Gln generates a catalytically inactive protein (K249Q hOGG1) that retains the ability to bind with nanomolar affinity and high specificity to DNA containing an oxoG:C base pair [7]. High-resolution X-ray structures [8, 9] of this stable recognition complex reveal a highly deformed DNA helix, with an abrupt 70° helical kink centered on the position of the extrahelical oxoG lesion. The protein enforces this deformed DNA structure through an extensive network of intimate contacts involving both the oxoG, the complementary C, and the helical segments flanking them. Importantly, oxoG:C base pairs induce no bend in DNA, as determined by X-ray [10] and NMR [11], though the thermal stability is comparable to that of A:T rather than G:C [12]. Hence, the sharply bent helical structure provides a readily discernible signature for tight contact between hOGG1 and DNA.

Results and Discussion

AFM Characterization of hOGG1 Bound at Oxo-G Sites

AFM has been shown to be especially useful in probing the structure of individual complexes of proteins and DNA [5, 13–15]. It is important to demonstrate that AFM visualization yields information that agrees well with conventional biochemical studies, since AFM studies require biomolecules to be deposited onto a surface. To show that the imaged molecules represent the equilibrium structure in solution, we first determined the persistence length of DNA on the surface by measuring the mean square end-to-end distance $\langle R^2 \rangle$ and then compared this with the equilibrium value predicted by the worm-like-chain model for molecules of the contour length L in two dimensions, in which $\langle R^2 \rangle = 4PL(1 - P/L[1 - e^{-L/2P}])$. The value obtained, 53 nm, matches bulk measurements in a similarly buffered environment as well as AFM studies with conventional probes [16]. The persistence length, as a measure of the intrinsic flexibility of DNA, can be used to predict the distribution of local bend angles (the angle by which DNA deviates from linearity at a local point). The bending energy for a DNA molecule modeled as a wormlike chain with persistence length P to be bent at an angle θ over a fragment of length l is $E_{bend} = Pk_BT\theta^2/2l$. The predicted standard deviation of the angle distribution in two dimensions for DNA fragments of 6 nm in length is thus $\sigma = (l/P)^{1/2} = 19.3°$. Our AFM imaging yielded a Gaussian distribution centered and folded at 0° with a standard deviation of 19° for the bending-angle distribution of native DNA stretches that were about 6 nm long. The excellent agreement between the experimentally measured and predicted values suggests that the intrinsic flexibility of the molecules dominates over measurement error as the origin of distribution width in our experiments.

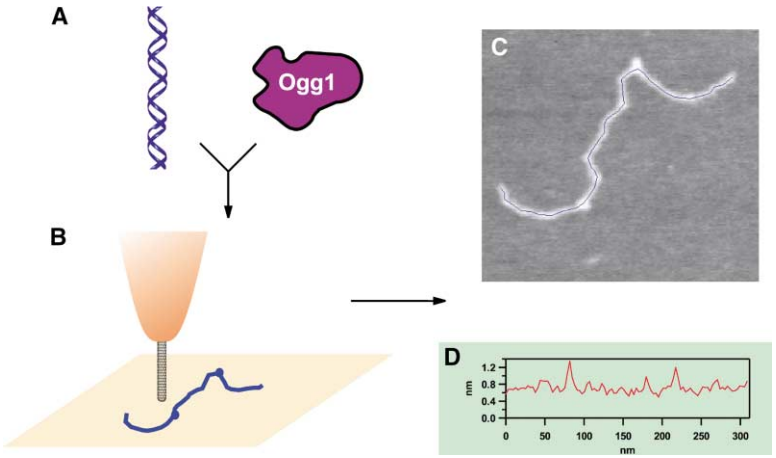

Figure 1. Experimental Strategy for Studying hOGG1 Target Searching by AFM with Carbon Nanotube Probes

A restriction fragment of a DNA plasmid is mixed with hOGG1 protein (A) and deposited onto a freshly cleaved mica surface where it is imaged with a nanotube probe (B). The resulting image (C) displays the conformation of the DNA at sites where the protein is bound. The height profile (D) is used for analyzing the binding site statistics.

We directly visualized recognition complexes between hOGG1 and DNA that contain a single oxoG:cytosine base pair in a defined location. The hOGG1-DNA complexes are readily observed in AFM images (Figures 2A and 2B). The footprint of hOGG1 on DNA is about 5 nm, which falls within the expected range based on the crystal structures [8, 9] and the minimal tip-broadening effect from nanotube AFM probes. Significantly, we observed a prevalence of structures in which DNA is drastically bent at the sites where hOGG1 is bound. To quantitatively characterize hOGG1 binding behavior, we measured the location of hOGG1 binding sites on a large number of complexes. The resulting histogram (Figure 2C) was fit to a Gaussian function centered at 79 nm with a standard deviation of 11 nm. This agrees well with the known oxoG location, 245 bp from one end

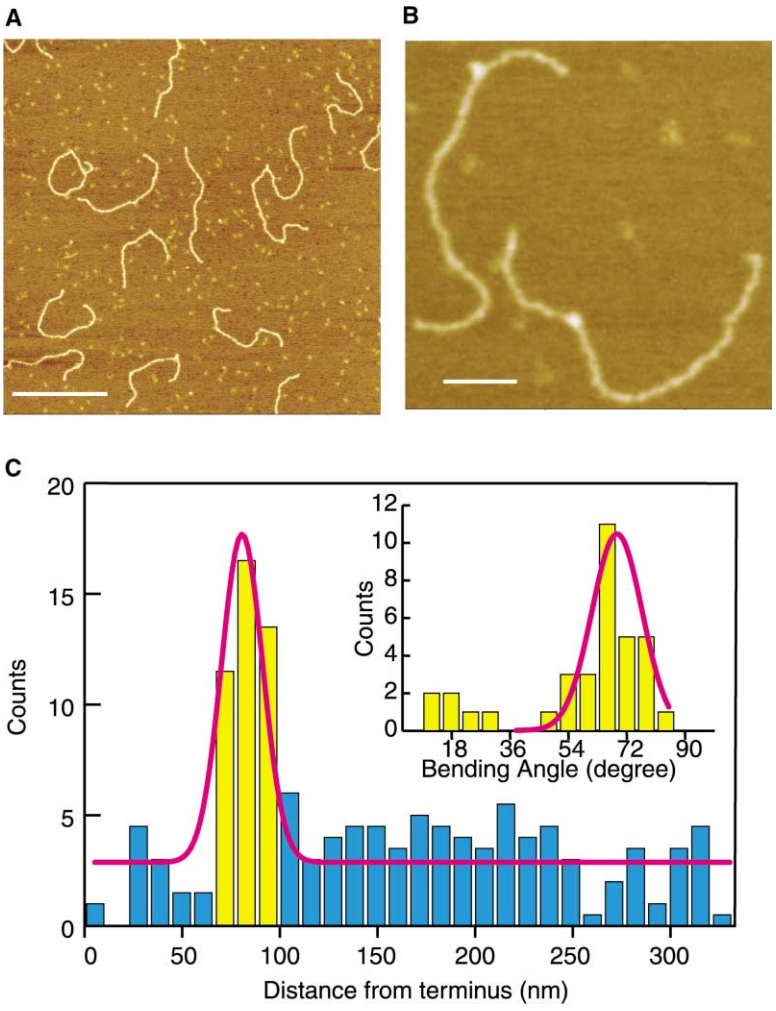

Figure 2. AFM Images and Analysis of the K249Q Mutant of hOGG1 Binding to a 1024 bp DNA Fragment Containing a Single oxoG that is Located at 245 bp from One End

(A and B) AFM images showing the hOGG1-DNA complexes. The white bar represents the length scale (A, 250 nm and B, 50 nm).

(C) Binding site distribution of hOGG1 on the 1024 bp DNA fragment containing a single oxoG 245 bp from one end. The blue bars correspond to nonspecific complexes and the yellow bars to specific complexes. The red line depicts a Gaussian fit to the data (mean = 79 nm, standard deviation = 11 nm) added to a constant background of 2.9 counts. The inset shows the bend angle distribution of the specific hOGG1-DNA complexes. The red line in the inset is a Gaussian fit to the bend angle data (mean = 71°, standard deviation = 9.2°). The minor peak around 0° may arise from hOGG1 nonspecific binding to base pairs adjacent to oxoG, or linear complexes at the specific oxoG site. The latter possibility is less likely but cannot be excluded based on detailed analysis.

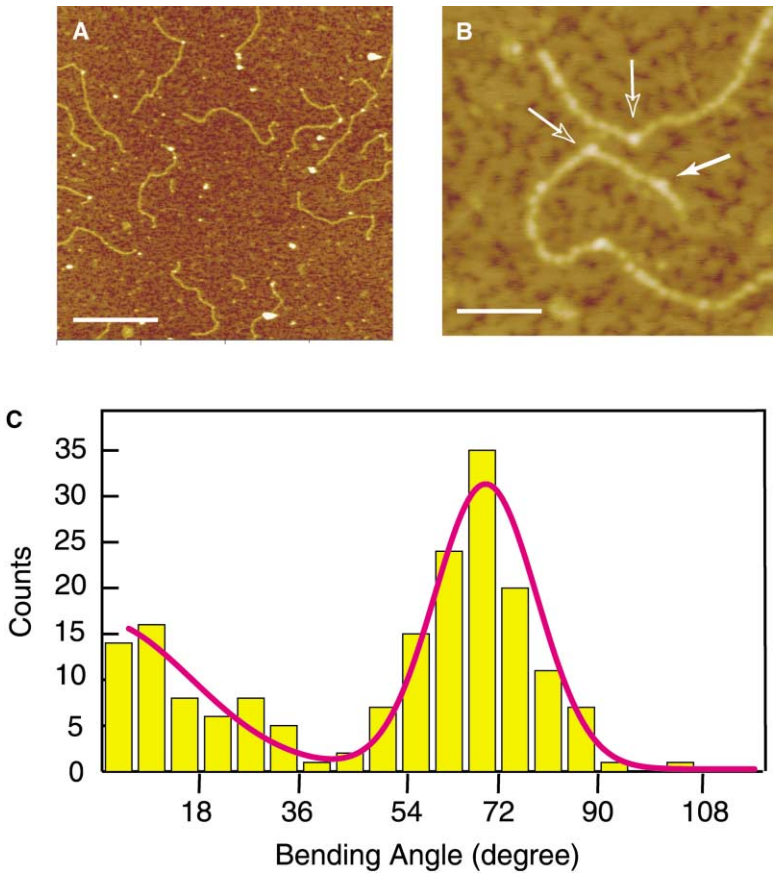

Figure 3. Native DNA Binding by Wild-Type hOGG1

(A and B) AFM images of wild-type hOGG1 bound to a 1234 bp native DNA fragment (no oxoG specifically introduced). Open and closed arrows in (B) denote bent and linear hOGG1-DNA complexes, respectively. The white bar represents the length scale (A, 250 nm; B, 50 nm).

(C) Bend angle distribution for native DNA with wild-type hOGG1. The red line depicts the calculated fit to the data, made by summation of a Gaussian centered around 70°(standard deviation = 9.3°) and a Gaussian centered and folded at 0°(standard deviation = 21°).

(corresponding to approximately 78 nm). The constant background in the binding-location histogram corresponds to hOGG1 binding to nonspecific DNA. The ratio of specific versus nonspecific binding was estimated by integration to be 1:2.5. Considering the relative abundance of nonspecific sites, we estimate that the binding affinity of K249Q hOGG1 for the oxoG lesion in DNA is approximately 400 times higher than that for unmodified sites in DNA. This difference is comparable to that observed in solution (S.D. Bruner, D.P. Norman, and G.L.V., unpublished data). We confirmed the validity of our location analysis by repeating the experiment with a 1349 bp DNA fragment, in which a single oxoG site was engineered at 549 bp from one end. The resulting images showed that K249Q hOGG1 clustered at a site that was 175 nm from one end of this molecule.

The distribution of the DNA bend angle at specific oxoG bound sites was also measured for individual complexes (Figure 2C, inset) and shows a clear clustering around 71° and a small peak close to 0° (see Figure 2C legend). Importantly, the predominant 71° angle for the hOGG1-DNA-specific complex matches the geometry observed in the cocrystal structures of hOGG1 and DNA [8, 9], providing further validation that AFM faithfully captures the overall structure of the glycosylase-DNA complex.

AFM Imaging of Search Intermediates at Undamaged Sites

Central to the results of this report are our images of hOGG1 on undamaged, native DNA. These images directly address the target-searching mechanism because such intermediates can be unambiguously identified and observed. Wild-type hOGG1 was mixed with native DNA and imaged. The DNA used in these experiments was freshly isolated from bacteria and was found to contain undetectable levels of oxoG. Significantly, a large number of bent complexes were observed in our AFM experiments (Figures 3A and 3B). These sharp bends appear similar to specific oxoG-hOGG1 complexes and can readily be distinguished from bends due to intrinsic flexibility of DNA. The bend angle distribution for these samples (Figure 3C) shows a bimodal distribution. Two-thirds of the complexes have the same bend angle as the specific complexes, even though no oxoG is present, and the remaining complexes are linear. A simple estimation of the elastic energy required for bending the helix by 70° based on the measured chain flexibility of DNA yields an energy of 8 kT at room temperature, which exceeds the available thermal energy. Therefore, the bending must result from the interaction between hOGG1 and DNA in the nonspecific complex. This constitutes the first direct evidence that hOGG1 bends nonspecific sites in searching for oxoG and that this bend angle is the same as for specific oxoG sites. The observed bimodal distribution of angles differs from previous AFM studies on protein-DNA interactions in which a single peak in the angle distribution, either bent or straight but not both coexisting, is observed [14, 15].

The bimodal distribution suggests that two populations of intermediates are in equilibrium during the search process, leading us to propose a framework for

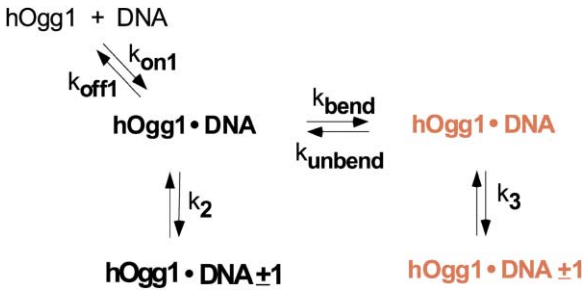

Figure 4. Schematic of the Proposed Kinetic Pathways for the hOGG1 Target-Searching Process

Initially, free hOGG1 binds to DNA nonspecifically to form the complex hOGG1•DNA. In this state, hOGG1 can freely diffuse along the DNA or make a structural transition to bent hOGG1•DNA (in red). It is not known whether it is kinetically more favorable for the bend in the DNA to directly propagate ($k_3 > k_{unbend}$) or for the bent complex to convert back to linear hOGG1•DNA before moving to an adjacent site ($k_3 < k_{unbend}$).

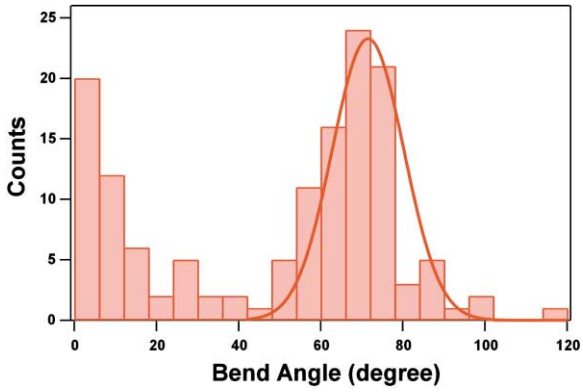

Figure 5. Bend Angle Distribution for Native DNA Bound with AlkA

The peak corresponding to bent complexes was fit to a Gaussian distribution centered around 72° with a standard deviation of 9°.

the hOGG1 target search model (Figure 4). We envision that in the first step, the protein, guided by the electrostatic interaction between the negatively charged phosphate backbone and the substantial α-helical dipole moments, binds to DNA [8]. The initial attachment to DNA reduces the dimensionality of the search by allowing facilitated one-dimensional diffusion [17]. We reason that, analogous to the sliding complexes postulated for T4 endonuclease V [18] and *E. coli* uracil DNA glycosylase (UDG) [19, 20], the resulting complex has little specific interaction between the protein and DNA. In this mode, the DNA conformation would not be significantly affected by hOGG1 binding, and this mode would therefore correspond to the observed linear complexes. Next, a structural transition occurs as new, extensive contacts between hOGG1 and DNA are used to force the DNA into a bent structure. This two-step binding model may be very similar to that which Stivers and coworkers proposed for *E. coli* UDG based on time-dependent changes in tryptophan fluorescence [21]. In the absence of oxoG, the thermodynamic free energy of the complex with hOGG1 at one particular site should be almost identical to hOGG1 bound at a neighboring site. Therefore, hOGG1 could translate to an adjacent site by one of three mechanisms: (i) unbending, sliding nonspecifically, and rebending; (ii) directly propagating the bent complex; or (iii) releasing the DNA and rebinding at an adjacent site.

Significantly, these single molecular-imaging results can be used for the evaluation of many of the critical microscopic equilibrium constants diagrammed in Figure 4. We estimate the equilibrium constant under AFM imaging conditions to be $K_1 = k_{on1}/k_{off1} = 2.2 \times 10^4\ M^{-1}$. The equilibrium constant $K_{bend} = k_{bend}/k_{unbend}$ is estimated to be 2 from the integration of the relative population of the two types of hOGG1-DNA complexes for native DNA (Figure 3C). Equilibrium constants K_2 and K_3 are expected to be 1 if sequence context effects are neglected. The kinetic rate constants cannot be obtained by imaging molecular snapshots. However, a time course in which the pre-deposition incubation time was varied showed that the average number of bound hOGG1 proteins per DNA molecule and the relative abundance of linear versus bent complexes reached their equilibrium values within 1 min (L.C., K.A.H., C.M.L., and G.L.V., unpublished data). Future studies involving the real-time in situ AFM imaging of hOGG1-DNA complexes in fluid could provide further knowledge about the dynamics of the search mechanism.

Implications for the Search Mechanism

The pivotal question surrounding the search mechanism is how hOGG1 accomplishes the daunting task of discriminating accurately against the nonmodified DNA bases. The observed bimodal distribution in bend angles excludes the possibility that the protein recognizes static conformation or dynamic flexibility of the DNA locus being searched because the 70° bend angle is not observed in the position of oxoG without the protein and, furthermore, hOGG1 is able to bend the duplex to 70° at many, if not all, sites along the DNA molecules whether or not oxoG is present. Can it be the case that the single hydrogen bond observed in the crystal structure between the main chain carbonyl of Gly42 and the N^7-H of an extrahelical oxoG is the determing factor? If so, does this require nontarget bases to be flipped out by hOGG1 [22]? We reason that the scanned base in the bent hOGG1-DNA complexes observed by AFM is likely to be extrahelical rather than intrahelical because a significant number of the protein-DNA contacts responsible for generation of the bend observed in the X-ray structures [8, 9] are entirely dependent upon the presence of an extrahelical base. An intrahelical model would require an entirely different set of intimate contacts between the DNA and the active site region of the protein and would coincidentally produce a bend of 70°. Thus, we envision that the protein-induced DNA bend allows hOGG1 to interrogate the DNA and that hOGG1 uses the same network of contacts observed in the crystal structure to enforce the bend and discriminate oxoG:C from normal base pairs. It has not proven possible to use fluorescent measurements to detect normal bases being flipped out of the duplex by DNA glycosylases *E. coli* UDG [21] or T4 endonuclease V [23]. However, *E. coli* AlkA, a glycosylase in the same HhH-GPD superfam-

ily [24] as hOGG1, has been shown to excise normal bases at a low but significant rate [25], consistent with the notion that the enzyme samples normal bases in the extrahelical active site.

Using the same AFM techniques applied to the hOGG1-DNA complexes, we found that the bend angle distribution for AlkA bound to native DNA also shows a bimodal distribution with a population of linear complexes and a large number of bent complexes (Figure 5). The observed 72° bend angle is similar to the 66° angle reported for the complex of AlkA bound to a damaged base analog [26]. Thus, the bimodal distribution of bend angles for nonspecific DNA binding is shared by at least two members of the HhH-GPD superfamily [24]. These results suggest that a key mechanistic step in the search process of these glycosylases probably involves swiveling of DNA bases into the enzymes' concave active pocket, where subtle base modifications can be detected.

Significance

Our experiments represent an important step forward in understanding the long-standing question of how DNA glycosylases search for their target lesions. We observe that hOGG1 bends DNA at undamaged bases. Preliminary experiments with AlkA suggest that this phenomenon may in general apply to other DNA repair enzymes, at least those of the HhH-GPD super family [24]. The dramatic distortion of the DNA conformation appears to be a requisite step as hOGG1 surveys DNA for damaged bases. This single-molecule experiment has started to elucidate critical biological questions that are otherwise not readily addressable with conventional ensemble measurements.

Experimental Procedures

Preparation of Nanotube Tips

Single SWNT or small SWNT bundle tips were made by direct CVD growth on commercially available SPM probes (FESP, k = 1–5 N/m, Digital Instruments). Supported Fe-Mo catalysts were prepared as previously described [27]. Chemical vapor deposition was carried out in a 1 inch tube furnace at 800°C. Ethylene was supplied at 2 standard cm^3 (sccm) for 3 min with a background gas flow of 600 sccm argon and 400 sccm of hydrogen. The grown nanotube tips were shortened via the electrical etching method by grounding the tip while biasing a rough niobium sample in force calibration mode or imaging mode [4].

Sample Deposition and AFM Imaging

A solution of the DNA-protein complex was prepared by the dilution of both components to a final concentration of 0.5–2 nM DNA and approximately 400 nM protein in 5 mM $MgCl_2$, then deposited onto freshly cleaved mica for 1 min. The surface was rinsed in 2 ml of distilled water and dried under a stream of pure nitrogen gas before AFM imaging. Images were captured under ambient conditions in tapping-mode at 2 Hz line scan speed with tip resonance frequency of 60–80 kHz by the use of a Digital Instrument Multimode Nanoscope IIIa. The tip deflection amplitude in tapping is usually 10 nm. The recorded images were imported into the Igor Pro program (Wavemetrics). A height profile of DNA molecules traced by image-processing tools developed by Dimitri Vezenov and Jonathan Guyer was used for the identification of proteins on DNA. Specifically, local maximums that have height values between 0.9 and 1.2 nm were scored as protein-DNA complexes (Figure 1D). Tracing the profile of the DNA molecules with a series of contiguous lines and adding up the total lengths of these lines allowed measurement of the DNA contour length. The distance of a particular binding site to the end of the DNA molecule along the profile was also measured by the same method. The internal angle of the DNA backbone at a protein binding site was measured by recording the coordinates of three points, the binding site and two points that are approximately 5 nm upstream and downstream from the binding site along the DNA molecule.

Preparation of DNA Substrates

For preparation of the 1235 bp nonspecific DNA substrate, the phagemid pBS+ (Stratagene) was isolated from transformed *E. coli* and immediately digested with *AseI*. The 1235 bp fragment was purified by the standard agarose gel extraction protocol (Qiaquick Gel Extraction Kit, Qiagen) and modified to include an incubation of the gel slice at 50°C for 30 min. This was followed by ethanol precipitation and resuspension in TE buffer. To prepare the 1024 bp DNA substrate containing a single oxoG lesion, primer **1** (5′-GCCAAGCTCXGAATTAACCC-3′, X = oxoG) was synthesized, PAGE purified, and then phoshorylated by T4 polynucleotide kinase. Single-stranded template DNA was prepared by standard helper phage rescue of phagemid pBS+ (Stratagene). Single-stranded circular DNA was annealed to primer **1**, and the primer was then extended with T4 DNA polymerase in the presence of T4 DNA ligase to seal the remaining nick. The solution was concentrated and buffer exchanged according to the QIAquick PCR Purification protocol (Qiagen), and the DNA was digested with SapI and NdeI. The digest products were separated by preparative agarose gel electrophoresis, followed by extraction of the DNA from the excised gel slice with the Gel Extraction Kit (Qiagen), modified to include an initial incubation of the gel slice at 50°C for 30 min. The gel-purified DNA fragment (1024 bp) was then further purified by ethanol precipitation and was finally resuspended in TE buffer.

Overexpression and Purification of hOGG1 and AlkA Proteins

Full-length wild-type hOGG1 protein was overexpressed and purified according to a published protocol [7]. Full-length K249Q mutant hOGG1, purified by a similar protocol, was a gift from Derek P.G. Norman. Full-length wild-type AlkA was a gift from Orlando Schärer.

Received: October 15, 2001
Accepted: December 14, 2001

Acknowledgments

We thank D.P.G. Norman and O.D. Schärer for providing purified proteins; S.D. Bruner, D.P.G. Norman, C.-L. Cheung, and J. Hafner for helpful discussions; and K. Plummer and A. Ruthenberg for critical reading of the manuscript. K.A.H. thanks the Graduate Research Fellowship from the American Chemical Society, Division of Organic Chemistry. The research in the Verdine lab was supported by the National Institute of General Medical Sciences and the research in the Lieber lab was supported by the National Institutes of Health and the Air Force Office of Scientific Research.

References

1. Lindahl, T., and Wood, R.D. (1999). Quality control by DNA repair. Science *286*, 1897–1905.
2. Scharer, O.D., and Jiricny, J. (2001). Recent progress in the biology, chemistry and structural biology of DNA glycosylases. Bioessays *23*, 270–281.
3. Moerner, W.E., and Orrit, M. (1999). Illuminating single molecules in condensed matter. Science *283*, 1670–1676.
4. Hafner, J.H., Cheung, C.L., and Lieber, C.M. (1999). Direct growth of single-walled carbon nanotube scanning probe microscopy tips. J. Am. Chem. Soc. *121*, 9750–9751.
5. Woolley, A.T., Li Cheung, C., Hafner, J.H., and Lieber, C.M. (2000). Structural biology with carbon nanotube AFM probes. Chem. Biol. *7*, R193–R204.
6. Boiteux, S., and Radicella, J.P. (2000). The human OGG1 gene:

structure, functions, and its implication in the process of carcinogenesis. Arch. Biochem. Biophys. *377*, 1–8.

7. Nash, H.M., Lu, R., Lane, W.S., and Verdine, G.L. (1997). The critical active-site amine of the human 8-oxoguanine DNA glycosylase, hOgg1: direct identification, ablation and chemical reconstitution. Chem. Biol. *4*, 693–702.
8. Bruner, S.D., Norman, D.P., and Verdine, G.L. (2000). Structural basis for recognition and repair of the endogenous mutagen 8-oxoguanine in DNA. Nature *403*, 859–866.
9. Norman, D.P.G., Bruner, S.D., and Verdine, G.L. (2001). Coupling of substrate recognition and catalysis by a human base-excision DNA repair protein. J. Am. Chem. Soc. *123*, 359–360.
10. Lipscomb, L.A., Peek, M.E., Morningstar, M.L., Verghis, S.M., Miller, E.M., Rich, A., Essigmann, J.M., and Williams, L.D. (1995). X-ray structure of a DNA decamer containing 7,8-dihydro-8-oxoguanine. Proc. Natl. Acad. Sci. USA *92*, 719–723.
11. Oda, Y., Uesugi, S., Ikehara, M., Nishimura, S., Kawase, Y., Ishikawa, H., Inoue, H., and Ohtsuka, E. (1991). NMR studies of a DNA containing 8-hydroxydeoxyguanosine. Nucleic Acids Res. *19*, 1407–1412.
12. Plum, G.E., Grollman, A.P., Johnson, F., and Breslauer, K.J. (1995). Influence of the oxidatively damaged adduct 8-oxodeoxyguanosine on the conformation, energetics, and thermodynamic stability of a DNA duplex. Biochemistry *34*, 16148–16160.
13. Woolley, A.T., Guillemette, C., Cheung, C.L., Housman, D.E., and Lieber, C.M. (2000). Direct haplotyping of kilobase-size DNA using carbon nanotube probes. Nat. Biotechnol. *18*, 760–763.
14. Erie, D.A., Yang, G., Schultz, H.C., and Bustamante, C. (1994). DNA bending by Cro protein in specific and nonspecific complexes: implications for protein site recognition and specificity. Science *266*, 1562–1566.
15. Van Noort, J., Orsini, F., Eker, A., Wyman, C., De Grooth, B., and Greve, J. (1999). DNA bending by photolyase in specific and non-specific complexes studied by atomic force microscopy. Nucleic Acids Res. *27*, 3875–3880.
16. Bustamante, C., and Rivetti, C. (1996). Visualizing protein-nucleic acid interactions on a large scale with the scanning force microscope. Annu. Rev. Biophys. Biomol. Struct. *25*, 395–429.
17. von Hippel, P.H., and Berg, O.G. (1989). Facilitated target location in biological systems. J. Biol. Chem. *264*, 675–678.
18. Dowd, D.R., and Lloyd, R.S. (1990). Biological significance of facilitated diffusion in protein-DNA interactions. Applications to T4 endonuclease V-initiated DNA repair. J. Biol. Chem. *265*, 3424–3431.
19. Higley, M., and Lloyd, R.S. (1993). Processivity of uracil DNA glycosylase. Mutat. Res. *294*, 109–116.
20. Bennett, S.E., Sanderson, R.J., and Mosbaugh, D.W. (1995). Processivity of Escherichia coli and rat liver mitochondrial uracil-DNA glycosylase is affected by NaCl concentration. Biochemistry *34*, 6109–6119.
21. Stivers, J.T., Pankiewicz, K.W., and Watanabe, K.A. (1999). Kinetic mechanism of damage site recognition and uracil flipping by Escherichia coli uracil DNA glycosylase. Biochemistry *38*, 952–963.
22. Verdine, G.L., and Bruner, S.D. (1997). How do DNA repair proteins locate damaged bases in the genome? Chem. Biol. *4*, 329–334.
23. McCullough, A.K., Dodson, M.L., Scharer, O.D., and Lloyd, R.S. (1997). The role of base flipping in damage recognition and catalysis by T4 endonuclease V. J. Biol. Chem. *272*, 27210–27217.
24. Nash, H.M., Bruner, S.D., Scharer, O.D., Kawate, T., Addona, T.A., Spooner, E., Lane, W.S., and Verdine, G.L. (1996). Cloning of a yeast 8-oxoguanine DNA glycosylase reveals the existence of a base-excision DNA-repair protein superfamily. Curr. Biol. *6*, 968–980.
25. Berdal, K.G., Johansen, R.F., and Seeberg, E. (1998). Release of normal bases from intact DNA by a native DNA repair enzyme. EMBO J. *17*, 363–367.
26. Hollis, T., Ichikawa, Y., and Ellenberger, T. (2000). DNA bending and a flip-out mechanism for base excision by the helix-hairpin-helix DNA glycosylase, Escherichia coli AlkA. EMBO J. *19*, 758–766.
27. Hafner, J.H., Bronikowski, M.J., Azamian, B.R., Nikolaev, P., Rinzler, A.G., Colbert, D.T., Smith, K.A., and Smalley, R.E. (1998). Catalytic growth of single-wall carbon nanotubes from metal particles. Chem. Phys. Lett. *296*, 195–202.